Received: 19 January 2021 | Revised: 6 December 2021 | Accepted: 7 December 2021

DOI: 10.1002/mp.15437

RESEARCH ARTICLE

MEDICAL PHYSICS

Deep learning-based AI model for signet-ring cell carcinoma diagnosis and chemotherapy response prediction in gastric cancer

Cong Li[1,2] | **Yun Qin**[3] | **Wei-Han Zhang**[4] | **Hanyu Jiang**[3] | **Bin Song**[3] | **Mustafa R. Bashir**[5,6,7] | **Heng Xu**[8] | **Ting Duan**[3] | **Mengjie Fang**[1,2] | **Lianzhen Zhong**[1,2] | **Lingwei Meng**[1,2] | **Di Dong**[1,2] | **Zhenhua Hu**[1,2] | **Jie Tian**[1,2,9,10] | **Jian-Kun Hu**[4]

[1] School of Artificial Intelligence, University of Chinese Academy of Sciences, Beijing, China

[2] CAS Key Laboratory of Molecular Imaging, the State Key Laboratory of Management and Control for Complex Systems, Beijing Key Laboratory of Molecular Imaging, Institute of Automation, Chinese Academy of Sciences, Beijing, China

[3] Department of Radiology, West China Hospital, Sichuan University, Chengdu, Sichuan, China

[4] Department of Gastrointestinal Surgery and Laboratory of Gastric Cancer, State Key Laboratory of Biotherapy, West China Hospital, Sichuan University, and Collaborative Innovation Center for Biotherapy, Chengdu, Sichuan, China

[5] Department of Radiology, Duke University Medical Center, Durham, North Carolina

[6] Center for Advanced Magnetic Resonance Development, Duke University Medical Center, Durham, North Carolina

[7] Department of Medicine (Gastroenterology), Duke University Medical Center, Durham, North Carolina

[8] Department of Laboratory Medicine, Precision Medicine Center, State Key Laboratory of Biotherapy, West China Hospital, Sichuan University, Chengdu, Sichuan, China

[9] Beijing Advanced Innovation Center for Big Data-Based Precision Medicine, School of Medicine and Engineering, Beihang University, Beijing, China

[10] Engineering Research Center of Molecular and Neuro Imaging of Ministry of Education, School of Life Science and Technology, Xidian University, Xi'an, Shaanxi, China

Correspondence
Jian-Kun Hu, Department of Gastrointestinal Surgery and Laboratory of Gastric Cancer, State Key Laboratory of Biotherapy, West China Hospital, Sichuan University, and Collaborative Innovation Center for Biotherapy, No. 37 Guoxue Alley, Chengdu, Sichuan 610041, China.
Email: hujkwch@126.com
Jie Tian, Zhenhua Hu, and Di Dong, CAS Key Laboratory of Molecular Imaging, Institute of Automation, Chinese Academy of Sciences, No. 95 Zhongguancun East Road, Hai Dian District, Beijing 100190, China.
Email: jie.tian@ia.ac.cn; zhenhua.hu@ia.ac.cn; di.dong@ia.ac.cn

Cong Li, Yun Qin, Weihan Zhang, and Hanyu Jiang contributed equally to this work.

Funding information
National Key R&D Program of China, Grant/Award Numbers: 2017YFC1309100, 2017YFA0205200; National Natural Science Foundation of China, Grant/Award Numbers:

Abstract

Purpose: We aimed to develop a noninvasive artificial intelligence (AI) model to diagnose signet-ring cell carcinoma (SRCC) of gastric cancer (GC) and identify patients with SRCC who could benefit from postoperative chemotherapy based on preoperative contrast-enhanced computed tomography (CT).

Methods: A total of 855 GC patients with 855 single GCs were included, of which 249 patients were diagnosed as SRCC by histopathologic examinations. The AI model was generated with clinical, handcrafted radiomic, and deep learning features. Model diagnostic performance was measured by area under the receiver operating characteristic curve (AUC), sensitivity, and specificity, while predictive performance was measured by Kaplan–Meier curves.

Results: In the test cohort (n = 257), the AUC, sensitivity, and specificity of our AI model for diagnosing SRCC were 0.786 (95% CI: 0.721–0.845), 77.3%, and 69.2%, respectively. For the entire cohort, patients with AI-predicted high risk had a significantly shorter median OS compared with those with low risk (median overall survival [OS], 38.8 vs. 64.2 months, p = 0.009). Importantly, in pathologically confirmed advanced SRCC patients, AI-predicted high-risk status was indicative of a shorter overall survival (median overall survival [OS], 31.0 vs. 54.4 months, p = 0.036) and marked chemotherapy resistance, whereas

91959130, 81971776, 81902437, 81771924, 61622117, 81671759, 81930053, 81527805, 91959205; Beijing Natural Science Foundation, Grant/Award Numbers: L182061, Z20J00105, JQ19027; Beijing Nova Program, Grant/Award Number: Z181100006218046; 1.3.5 Project for Disciplines of Excellence, West China Hospital; Sichuan University, Grant/Award Number: ZYJC21006; Post-Doctor Research Project, West China Hospital, Sichuan University, Grant/Award Number: 2018HXBH010; China Postdoctoral Science Foundation, Grant/Award Numbers: 2019M653418, 2020T130449; Strategic Priority Research Program of Chinese Academy of Sciences, Grant/Award Number: XDB 38040200; Scientific Instrument Developing Project of the Chinese Academy of Sciences, Grant/Award Number: YZ201672; Youth Innovation Promotion Association CAS, Grant/Award Number: 2017175

AI-predicted low-risk status had substantial chemotherapy benefit (median OS [without vs. with chemotherapy], 26.0 vs. not reached, $p = 0.013$).

Conclusions: The CT-based AI model demonstrated good performance for diagnosing SRCC, stratifying patient prognosis, and predicting chemotherapy responses. Advanced SRCC patients with AI-predicted low-risk status may benefit substantially from adjuvant chemotherapy.

KEYWORDS
chemotherapy, deep learning, diagnosis, signet-ring cell carcinoma, survival

1 | INTRODUCTION

Gastric cancer (GC) is one of the most common cancers and is a major cause of cancer-related death globally.[1,2] Signet-ring cell carcinoma (SRCC) is defined as GC composed of at least 50% signet-ring cells in the pathologic specimen.[3] In prior studies, SRCC was exclusively found in the diffuse subtype of the Lauren classification of GC and was significantly associated with advanced tumor stage and a higher risk of metastasis.[4–6] Interestingly, while associated with better survival and prognosis in early GC, SRCC in advanced GC is an unfavorable histological subtype and is an independent prognostic factor for lymph node and distant metastases, increased chemotherapy resistance, and poor survival.[4–6]

Despite the prognostic significance of SRCC, preoperative diagnosis of SRCC still relies on tissue biopsies, which are invasive and subjective to sampling error.[7] These intrinsic limitations are exacerbated by the heterogenous nature of GC and thus may give rise to a biased diagnosis and delayed or even inappropriate treatment.[8] However, the field of noninvasive approaches for SRCC is in its infancy.[9,10] Therefore, a noninvasive and easy-to-use tool for predicting SRCC is necessary. Moreover, due to the uncertainty of the efficacy of chemotherapy in SRCC patients, an easy-to-use tool for predicting chemotherapy response and survival for SRCC patients is necessary.[6] The strengths of imaging, in particular the ability to assess the tumor in its entirety, are well suited to overcome the current challenges in SRCC diagnosis and prognosis.[11]

Based on medical imaging and artificial intelligence (AI), radiomics has become a hot research topic in cancer research.[12–16] Radiomics converts images into minable data and extracts high-dimensional quantitative features from these data.[17,18] These radiomic features, which include handcrafted features and deep-learning features, may reflect the pathological or physiological features of cancer. It should be mentioned that we termed the traditional radiomic features as handcrafted features for distinguishing them from deep learning features. Handcrafted and deep learning features can be assessed using AI analytical methods to assist personalized precision medicine.[19,20] Some studies have reported that handcrafted and deep learning features offer complementary information by which more accurate decisions can be made.[21,22] Radiomics has been widely used in cancer detection, diagnosis, and prognosis.[23,24] Specifically, the value of radiomics has been validated in the differentiation of pathologic types in GC.[25] However, there is no study to our knowledge utilizing a radiomics approach or AI to address the SRCC diagnosis and prognosis problem.

Therefore, we aimed to develop an AI model to diagnose SRCC and to stratify the risk of postoperative chemotherapy resistance and patient survival on preoperative contrast-enhanced CT.

2 | MATERIALS AND METHODS

Our institutional review board approved this secondary analysis, and the requirements for informed consent were waived because all patient data were retrospectively retrieved from a prospectively collected database (Surgical Gastric Cancer Patient Registry [SGCPR],[26,27] registration No.: WCH-SGCPR-2020-01).

2.1 | Patients

From June 1, 2009 to December 31, 2014, consecutive patients with primary GC who underwent gastrectomy in West China Hospital, Sichuan University had been enrolled in the gastric cancer registry. The inclusion criteria were as follows: (1) patients underwent partial or total gastrectomy with regional lymphadenectomy in two gastric cancer surgical treatment teams

and (2) patients with available contrast-enhanced CT scan of the abdomen within 30 days prior to surgery. Patient exclusion criteria were as follows: (1) with preoperative chemotherapy and/or radiotherapy; (2) underwent surgery for previous remnant gastric cancers; (3) incomplete CT image data for qualitative and/or quantitative analysis; and (4) lost to postoperative follow-up. Curative intent surgical resection had been performed according to the Japanese gastric cancer treatment guidelines 2010.[28] Postoperative chemotherapy based on 5-fluorouracil and oxaliplatin was recommended for patients at advanced T stages and/or with lymph node metastasis. All patients had been followed-up after surgery with CT or MRI at least twice per year in the first three years and once per year thereafter until death, loss of follow-up or 12/30/2019, whichever came first. Patients were randomly allocated to the training or test cohort at a 7:3 ratio.

2.2 | Histopathologic analysis

Histopathologic examinations of the resected specimens were used as the reference standard for SRCC diagnosis according to the WHO Classification of Tumors of the Digestive System, and patients were classified into SRCC (containing > 50% of signet-ring cells) or non-SRCC (containing < 50% of signet-ring cells in pathologic specimen).[3] Other pathological characteristics, including TNM stage and Lauren's classification were also collected.[29]

All histopathologic examinations were assessed independently by two pathologists who were aware of the clinical and imaging data. All disagreements were resolved by discussion and consensus.

2.3 | Imaging acquisition

Preoperative multiphasic contrast-enhanced CT scans were acquired using several multidetector CT scanners in this study. CT images were acquired before and after administration of contrast media during the arterial phase (AP) and portal venous phase (PVP). Detailed imaging acquisition protocols are summarized in Supplementary Material 1.

2.4 | Regions of interest (ROIs) segmentation

A study coordinator (*[BLINDED FOR REVIEW]*) with 6 years of experience in gastrointestinal imaging retrieved and de-identified all patient images, evaluated the image quality, and determined the locations of the gastric lesion on the maximum cross sections of PVP CT images with reference to the surgical and pathological reports.

All CT images were then reviewed independently by two abdominal radiologists (*[BLINDED FOR REVIEW]*) who were blinded to any clinicopathologic and follow-up information with 5 and 6 years of experience in gastrointestinal CT imaging, respectively. For each patient, a manually delineated tumor ROI (ROI_{tumor}) was placed by each reviewer along the entire tumor margin on the maximum cross sections of precontrast, AP, and PVP images. A minimum bounding rectangle ROI (ROI_{rec_tumor}) was automatically generated by computer to encompass the corresponding ROI_{tumor} for development of the deep learning models.

2.5 | Model development

First, we built individual models based on handcrafted radiomics, deep learning, and clinical features for predicting SRCC, respectively. Finally, an AI model that encompassed all of the above features was generated.

2.5.1 | Radiomics model

A total of 448 handcrafted features were extracted from each ROI_{tumor} using the Pyradiomics package (http://pyradiomics.readthedocs.io) in Python (version 3.6; https://www.python.org/).[30] Then, feature extraction was performed based on each radiologist's ROIs separately. During the feature selection, intraclass correlation coefficient (ICC), univariate analysis, minimum redundancy maximum relevance algorithm (mRMR), and backward stepwise according to Akaike's information criterion (AIC) were used to remove irrelevant features. Afterward, multivariate logistic regression was performed to construct a radiomics model ($Model_R$) based on the optimal feature subset. Detailed feature extraction and selection are described in Supplementary Material 2.

2.5.2 | Deep learning model

Additionally, we developed a deep learning model ($Model_{DL}$) to predict the SRCC directly from the images.

In order to extract specific characteristics of the primary tumor, we developed the deep learning model in the following two steps. First, we adopted U-Net as a semantic segmentation network and performed a segmentation task.[31,32] The input of the segmentation network was the ROI_{rec_turmor}. The ground truth was the binarized ROI_{tumor} (1: primary tumor, 0: other tissues). Both the input and the ground truth were first resized to 112 × 112 pixels by bilinear interpolation.

Second, we appended three fully connected layers behind the encoder network of U-Net and termed it as a classification network ($Model_{DL}$). The weight of $Model_{DL}$ was initialized by U-Net and fine-tuned for five epochs.[33] Consequently, $Model_{DL}$ could extract more specific characteristics of the primary tumor itself. All of the above operations were conducted in the training cohort.

During the training process, online sample augmentation techniques were used to improve model robustness, such as random rotation, horizontal flip, and vertical flip. For alleviating the issue of class balance, we adopted a weighted random sampler method in each batch. In addition, we randomly selected one-fifth of the training cohort samples as the validation set for hyperparameter optimization. More details of the image preprocessing, model structure, and hyperparameter are described in Supplementary Material 3.

2.5.3 | Clinical model

Preoperative clinical characteristics (patient age, gender, and tumor location) were fed into a logistic regression model to diagnose SRCC. A clinical model ($Model_C$) was established accordingly based on significant clinical characteristics selected by multivariate analyses.

2.5.4 | The combined AI model

Finally, a logistic regression algorithm was conducted to build $Model_{AI}$, combing significant medical features with the outputs of $Model_R$ and $Model_{DL}$. $Model_{AI}$ generated the probability that each patient belongs to SRCC. The development of the combined AI model is shown in Figure 1.

2.6 | Statistical analysis

Differences between two groups were estimated by an independent-sample *t*-test or Mann–Whitney *U* test for continuous variables and chi-square test or Fisher exact test for categorical variables.

The areas under the receiver operating characteristic curves (AUCs) were used to estimate model diagnostic performance and were compared by the Delong test. We selected thresholds by maximizing the Youden index in the training cohort, applied these thresholds to the testing cohort, and calculated accuracy, specificity, and sensitivity. Calibration curves were plotted to assess the calibration of the AI model and examined by the Hosmer-Lemeshow test. In addition, decision curve analysis was conducted to estimate the AI model's clinical usefulness by quantifying the net benefits at different threshold probabilities. We computed the net reclassification index (NRI) to assess diagnostic improvements between models. In order to measure model predictive performance and robustness, we performed fivefold cross-validation on the entire dataset and computed the mean AUC across all folds and relative standard deviation as a percentile (RSD, RSD = (sdAUC/meanAUC) × 100%).[34] Furthermore, stratification analysis was performed on patient age, gender, and tumor locations.

Kaplan–Meier curves were constructed to analyze overall survival (OS) outcomes, with the log-rank test used to assess statistical significance. Patients were stratified into high-risk and low-risk groups according to an optimal cutoff point estimated in the training cohort by X-tile software based on the probability scores of $Model_{AI}$ (version 3.6.1; Yale University School of Medicine, New Haven, CT, USA).[35]

All analyses were conducted with R software (version 3.5.1; http://www.Rproject.org). A two-sided $p < 0.05$ was used to indicate a statistically significant difference.

3 | RESULTS

3.1 | Histopathologic characteristics

A total of 855 patients (median age, 59.2 years; range, 21–86 years, 594 men) each with a single GC lesion (median size, 6.0 cm, range, 1.0–25.0 cm) were included. Consistent with previous reports, patients with SRCC ($n = 249$, 29.1%) were younger and more likely to be female than those with non-SRCC (Table 1). SRCC was also more frequently found in the nonesophagogastric junction of the stomach, in the diffuse subtype of Lauren's classification, and associated with more advanced pathological T, N, and M stages (Table 1). Among these patients, 598 (69.9%) were assigned to the training cohort and 257 (30.1%) were assigned to the test cohort (Figure 2). No difference in any clinical characteristics was observed between the training and test cohorts (Supplementary Material 4).

3.2 | Diagnostic performance of different models

3.2.1 | Radiomics model

We constructed models with features from precontrast, AP, and PVP phases, respectively. Because no significant improvement was achieved after combining features derived from precontrast and AP images, four features from PVP exclusively (detailed in Supplementary Material 5) were used to generate $Model_R$. The AUC for $Model_R$ was 0.697 (95% confidence interval [CI]: 0.648–0.744) in the training cohort and 0.700 (95% CI: 0.617–0.777) in the test cohort, respectively (Table 2 and Figure 3).

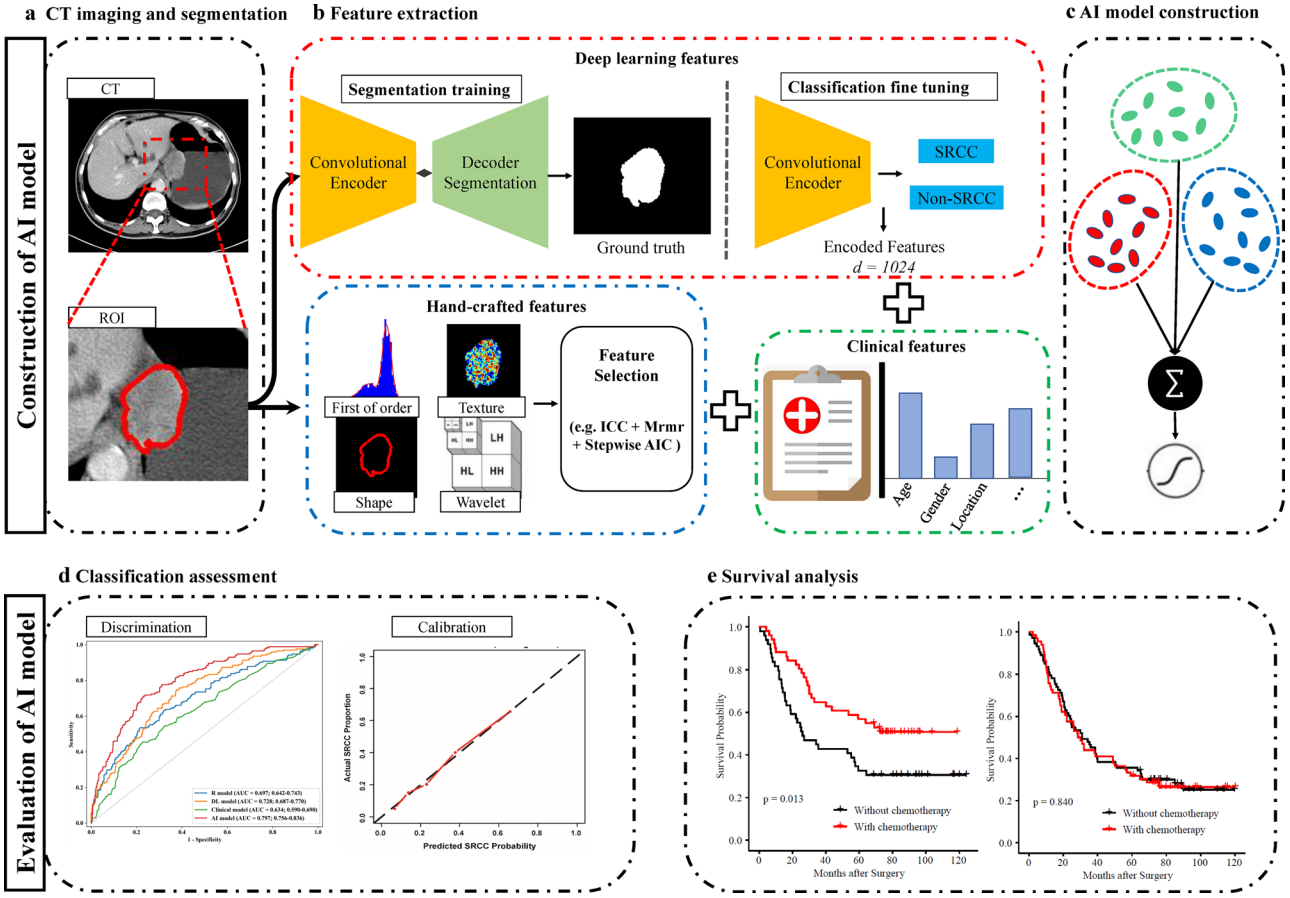

FIGURE 1 The pipeline of AI model construction and assessment. (a) Original CT images and segmentation of the region of interest by two radiologists. (b) Deep learning and handcrafted feature extraction from the primary tumor. (c) Construction of AI model based on deep learning, handcrafted, and clinical features. (d), (e) Evaluation of the AI model in SRCC classification and stratification. R model, radiomics model; DL model, deep learning model

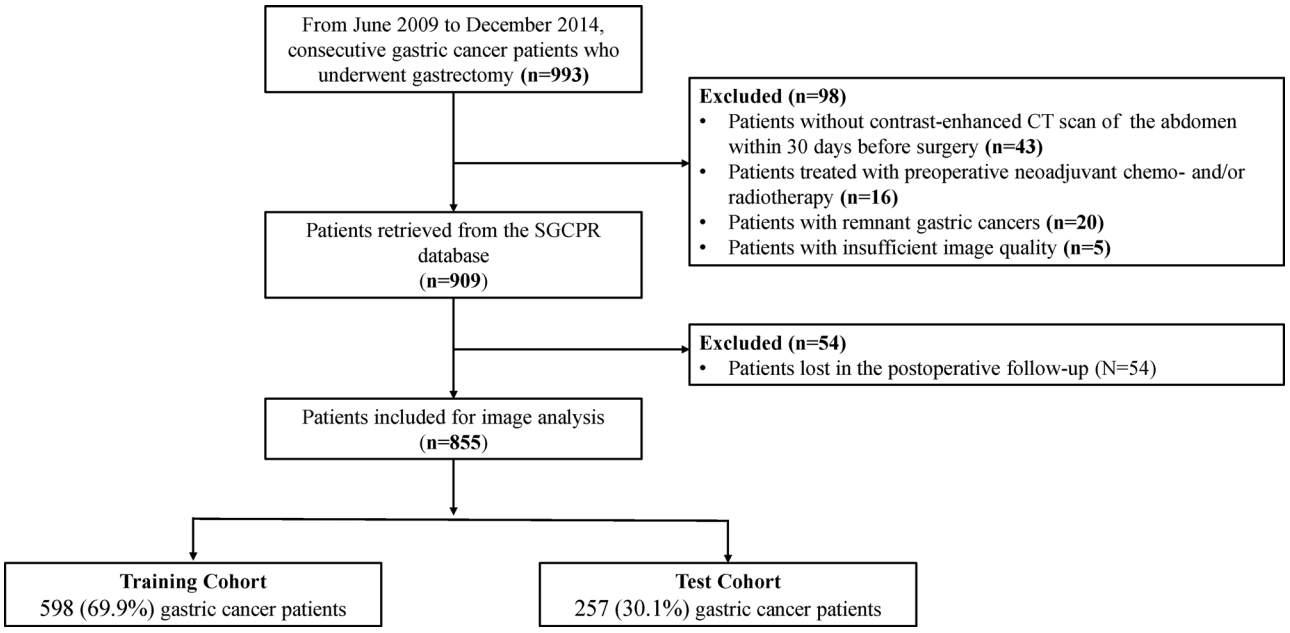

FIGURE 2 Process of patient enrollment for training and test cohorts. SGCPR, Surgical Gastric Cancer Patient Registry

TABLE 1 Characteristics of GC patients in this study

Characteristics	SRCC	Non-SRCC	*p* Value*
No. of patients	249	606	…
Median age (range in years)	57 (21–84)	61 (26–86)	<0.001*
Gender no. (%)			<0.001*
Male	142 (57.0)	452 (74.6)	
Female	107 (43.0)	154 (25.4)	
Tumor size median (range in mm)	7.0 (1.0–25.0)	6.0 (1.0–25.0)	<0.001*
Lauren classification no. (%)			<0.001*
Intestinal subtype	3 (1.2)	170 (28.1)	
Diffuse subtype	186 (74.7)	110 (18.2)	
Mixed subtype	20 (8.0)	82 (13.5)	
Unknown	40 (16.1)	244 (40.2)	
Tumor location no. (%)			<0.001*
Esophagogastric junction	57 (22.9)	219 (36.1)	
Other locations	192 (77.1)	387 (63.9)	
T stage no. (%)			0.01*
pT1 stage	8 (3.2)	27 (4.5)	
pT2 stage	17 (6.8)	69 (11.4)	
pT3 stage	30 (12.0)	108 (17.8)	
pT4 stage	194 (78.0)	402 (66.3)	
N stage no. (%)			<0.001*
pN0 stage	30 (12.0)	119 (19.6)	
pN1 stage	22 (8.8)	103 (17.0)	
pN2 stage	36 (14.5)	124 (20.5)	
pN3 stage	161 (64.7)	260 (42.9)	
M stage no. (%)			0.024*
pM0 stage	202 (81.1)	528 (87.1)	
pM1 stage	47 (18.9)	78 (12.9)	
No. of patients with adjuvant chemotherapy (%)			0.368
With adjuvant chemotherapy	121 (48.6)	315 (52.0)	
Without adjuvant chemotherapy	128 (51.4)	291 (48.0)	

Note. Unless stated otherwise, data are the number of patients or lesions. Data are presented as count (percentage), mean ± standard deviation, or median (range), where applicable.

*Comparisons are made using the Student's *t*-test or Mann–Whitney *U* test for continuous variables, and with the χ^2 test or Fisher's exact test for categorical variables, where applicable. SRCC, signet-ring cell carcinoma.

TABLE 2 Model diagnostic performance for signet-ring cell carcinoma

	Training cohort				Test cohort			
Index	**AUC (95% CI)**	**ACC**	**SEN**	**SPE**	**AUC (95% CI)**	**ACC**	**SEN**	**SPE**
Model$_C$	0.634 (0.586–0.689)	68.1%	45.4%	77.4%	0.640 (0.559–0.717)	68.1%	40.0%	79.7%
Model$_R$	0.697 (0.648–0.744)	64.7%	64.4%	64.9%	0.700 (0.617–0.777)	65.0%	62.7%	65.9%
Model$_{DL}$	0.728 (0.681–0.768)	65.9%	74.7%	62.3%	0.716 (0.641–0.780)	63.8%	70.7%	61.0%
Model$_{AI}$	**0.797** (0.763–0.840)	72.2%	73.0%	71.9%	0.786 (0.721–0.845)	71.6%	77.3%	69.2%

ACC, accuracy; SEN, sensitivity; SPE, specificity; AUC, area under curve; CI, confidence interval.

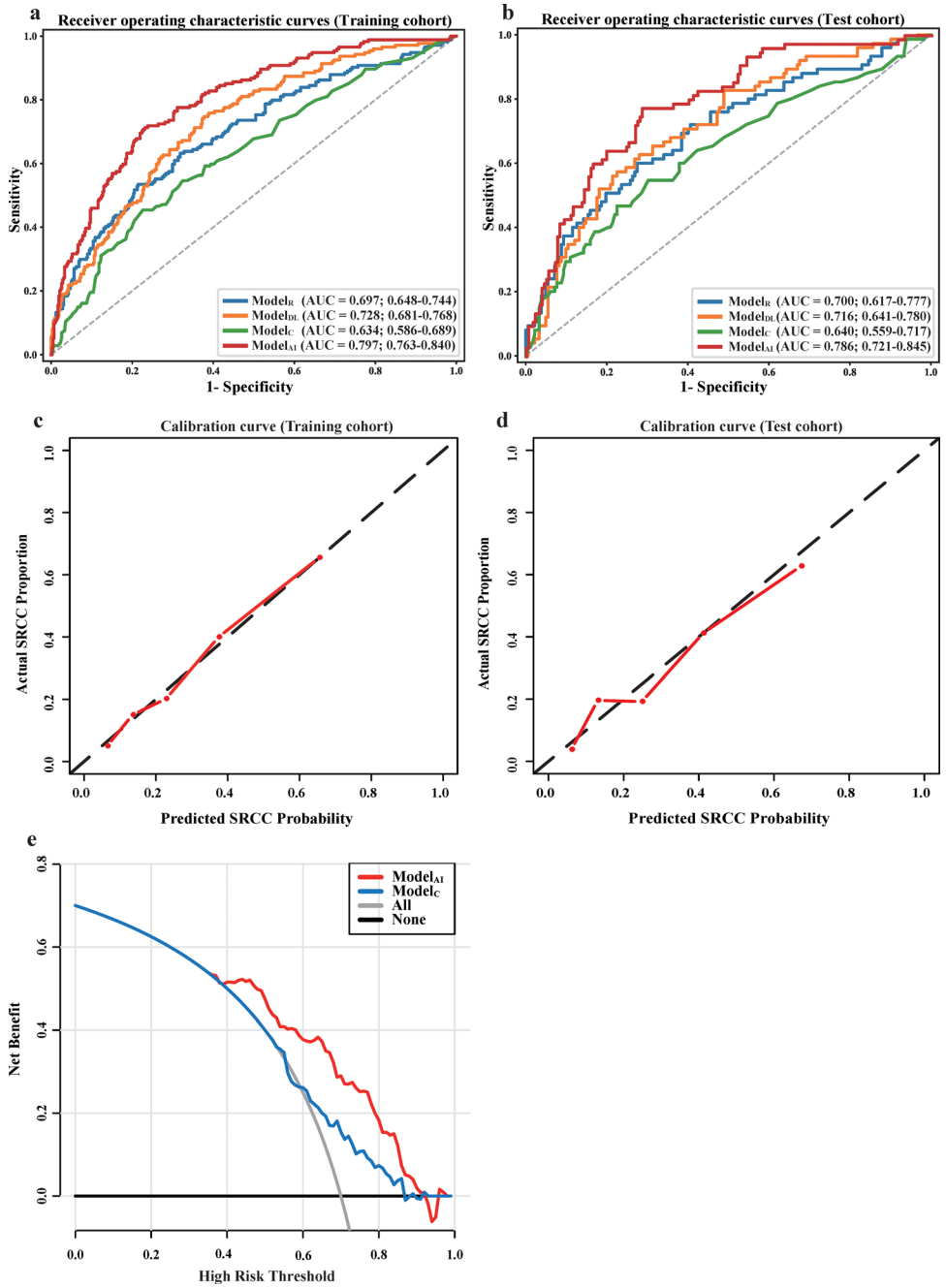

FIGURE 3 Receiver operating characteristic curves, calibration curves, and decision curves of SRCC diagnose by different models. (a), (b) Receiver operating characteristic curves of the radiomics ($Model_R$), deep learning ($Model_{DL}$), clinical ($Model_C$), and AI ($Model_{AI}$) models in the training and test cohorts. (c), (d) Calibration curves of $Model_{AI}$ in the training and test cohorts. (e) Decision curves of $Model_{AI}$, $Model_C$, all-diagnosed-as-SRCC, and all-diagnosed-as-non-SRCC. SRCC, Signet-ring cell carcinoma

3.2.2 | Deep learning model

Similarly, as precontrast and AP images did not bring in additional diagnostic benefits, $Model_{DL}$ was constructed solely on PVP images (Supplementary Material 5). $Model_{DL}$ yielded an AUC of 0.728 (95% CI: 0.681–0.768) in the training cohort and 0.716 (95% CI: 0.641–0.780) in the test cohort, respectively.

3.2.3 | Clinical model

Only patient age (odds ratio [OR] = 0.975, $p = 0.001$) and gender (OR = 1.992, $p = 0.001$) were identified as significant predictive clinical factors for SRCC in the multivariate analysis in the training cohort. $Model_C$, which incorporated only these two factors, demonstrated an AUC of 0.634 (95% CI: 0.586–0.689) in the training

cohort and 0.640 (95% CI: 0.559–0.717) in the test cohort (Table 2 and Figure 3).

3.2.4 | The combined AI model

After integrating the outputs of $Model_R$ and $Model_{DL}$ and significant clinical features, $Model_{AI}$ had the highest AUCs of 0.797 (95% CI: 0.763–0.840) in the training cohort and 0.786 (95% CI: 0.721–0.845) in the test cohort, respectively (Table 2 and Figure 3). According to the cross-validation experiments, the mean AUC of $Model_{AI}$ was 0.780 (range: 0.738–0.833) and RSD = 4.57% in the test cohort, indicating satisfactory method robustness. The calibration curve (Figure 3) demonstrated good agreement between predicted and observed SRCC in both the training ($p = 0.84$) and test cohorts ($p = 0.45$). As indicated by the stratification analysis, performance of $Model_{AI}$ was not affected by patient age ($p = 0.67$), sex ($p = 0.80$), or tumor location ($p = 0.20$) (Supplementary Material 6).

3.2.5 | Comparisons between models

In the test cohort, $Model_{AI}$ performed significantly better than $Model_R$ (Delong test: $p = 0.002$; NRI: 0.180, $p = 0.006$), $Model_{DL}$ (Delong test: $p = 0.005$; NRI: 0.196, $p = 0.001$), and $Model_C$ (Delong test: $p < 0.001$; NRI: 0.260, $p < 0.001$), and similar results were also found in the cross-validation experiments ($p < 0.05$ for all pairwise comparisons, Supplementary Material 7). When the above models were used for preoperative SRCC prediction, the decision curves also revealed the greatest benefit for $Model_{AI}$ (Figure 3).

3.3 | Prediction of postoperative survival

A total of 851 (99.5%) patients had complete OS follow-up information until 12/30/2019, with overall death rate of 57.2% (487/851). The median OS of these patients was 53.6 (95% CI: 43.8–66.7) months and was 38.2 (95% CI: 30.0–55.2) months for SRCC patients and 66.7 (95% CI: 48.7–87.7) months for non-SRCC patients (log-rank $p = 0.003$). Utilizing $Model_{AI}$ to stratify patients into high-risk and low-risk groups according to the optimal cutoff point determined by X-tile software, the median OS was 38.8 (95%CI: 31.0–56.0) months for high-risk patients and 64.2 (95% CI: 47.8–85.8) months for low-risk patients (log-rank test $p = 0.009$) (Supplementary Material 8). The pathologically determined SRCC status and the probability scores of $Model_{AI}$ yielded comparable performance in predicting OS.

We further explored the utility of $Model_{AI}$ in predicting survival and the chemosensitive profiles in patients with pathologically confirmed advanced (T2–T4 stages) SRCC ($n = 239$). We found that advanced SRCC patients with AI-predicted high risk ($n = 139$) had significantly shorter median OS compared with those with low risk ($n = 100$) (31.0 months vs. 54.4 months, log-rank $p = 0.036$). In addition, chemotherapy benefit was insignificant in the whole advanced SRCC patients (median OS [without vs. with chemotherapy], 30.5 vs. 43.6, $p = 0.110$). Furthermore, we evaluated whether AI-predicted risk status could predict adjuvant chemotherapy response. Not surprisingly, chemotherapy benefit was substantial in the AI-predicted low-risk group (median OS [without vs. with chemotherapy], 26.0 vs. not reached, $p = 0.013$), while insignificant in the high-risk group (median OS [without vs. with chemotherapy], 31.0 vs. 29.3, $p = 0.840$).

The survival analysis results are summarized in Table 3, and the Kaplan–Meier curves are shown in Figure 4 and Supplementary Material 9.

4 | DISCUSSION

Accurate and noninvasive assessment of SRCC, a factor associated with paradoxical prognosis in early (characterized by better survival) and advanced (characterized by increased chemotherapy resistance and worse survival) GCs, is paramount for personalized management. Based on a large-scale GC cohort, we generated a noninvasive CT-based preoperative promising AI model integrating clinical, handcrafted radiomics and DL features, which showed good diagnostic accuracy for SRCC. Our study was, to our knowledge, the first attempt to investigate the value of AI in preoperative SRCC diagnosis. Our predictive models demonstrated potential value in predicting long-term survival and, more importantly, treatment response to standard chemotherapies for SRCC.

Several GC subtyping systems have been introduced to stratify patient survival and guide treatment decision-making, but most of these systems require invasive histopathological evaluations. Promising results have been reported on the utility of imaging techniques,[36,37] particularly with the assistance of AI, in discriminating between Lauren's subtypes (e.g. diffuse vs. intestinal subtypes). However, among all subtyping systems of GC, SRCC has been identified as a particularly informative prognostic factor indicative of poor patient survival and increased chemotherapy resistance at advanced stages. Conventional CT features of GC, including enhancement pattern and tumor thickness, have been indicative of SRCC.[38] However, these features were subjective, nonspecific, and with limited diagnostic utilities. In contrast, AI techniques hold great promise in revealing intrinsic tumor biology unseen by human eyes and hence may overcome the barriers posed by conventional imaging evaluations. The AI model

TABLE 3 Survival analysis in GC patients

Cohort	Group	Median (months)	95% CI (months)	Log-rank test *p*
All patients	SRCC	38.2	30.0–55.2	0.003
	Non-SRCC	66.7	48.7–87.7	
All patients	AI-predicted high risk	38.8	31.0–56.0	0.009
	AI-predicted low risk	64.2	47.8–85.8	
Advanced SRCC patients	AI-predicted high risk	31.0	30.0–not reached	0.036
	AI-predicted low risk	54.4	24.4–39.8	
Advanced SRCC patients	With adjuvant chemotherapy	43.6	30.0–69.0	0.110
	Without adjuvant chemotherapy	30.5	24.0–40.0	
Advanced SRCC patients with AI-predicted low risk	With adjuvant chemotherapy	Not reached	43.3–not reached	0.013
	Without adjuvant chemotherapy	26.0	18.7–59.4	
Advanced SRCC patients with AI-predicted high risk	With adjuvant chemotherapy	29.3	21.1–53.0	0.840
	Without adjuvant chemotherapy	31.0	24.0–50.4	

SRCC, signet-ring cell carcinoma; AI, artificial intelligence.

demonstrated good discrimination and calibration performance for SRCC diagnosis, which underscored its promising potential in depicting the histologic profiles of GC.

We investigated the effects of SRCC status and the AI model in GC prognosis stratification in our cohort. In parallel with prior studies,[4,39,40] SRCC confirmed at postoperative pathology was associated with a more unfavorable prognosis in advanced GCs, as was the case with the AI model. However, despite being indicative of a poor prognosis, few treatment options are available to improve the long-term survival of advanced SRCC patients after gastrectomy, and the therapeutic benefit of chemodrugs remains a current matter of debate. Fortunately, as put forth in a bi-center study,[41] around 16.3% locally advanced esophagogastric SRCCs could achieve survival benefits after neoadjuvant chemotherapy, highlighting the importance of finding biomarkers, which may help identify potential chemoresponders in this specific population. For this purpose, previous genomics studies reported that somatic alteration of *CLDN18-ARHGAP26* fusion was detected in predominantly diffuse gastric cancers indicating its unique role.[42] The value of *CLDN18-ARHGAP26* fusion was further confirmed in another study as a promising indicator of a more unfavorable prognosis and increased chemodrug resistance in patients with advanced SRCC.[39] However, the utility of this fusion gene remains in the preclinical domain, largely because its evaluation is still mandated by the histological analysis of the resected tumor tissues, which were variegated at genomic and phenotypic levels.

In contrast, by characterizing a much larger area of the primary tumor than a biopsy, noninvasive imaging techniques are well suited to address the intrinsic tension between the tumor heterogeneity and limited sample tissues acquired at biopsy. Early gastric cancer patients are mostly treated by endoscopic resection, while advanced gastric cancer patients are mostly treated with chemotherapy.[28] However, SRCC is significantly associated with advanced tumor stage and is an independent prognostic factor for increased chemotherapy resistance and poor survival.[4,5] Therefore, we explored whether our AI model could help in stratifying advanced SRCC patients into subgroups with different treatment outcomes to derive similar results. In the current study, advanced SRCC patients with AI-predicted high risk had a markedly worse survival compared with those with a low risk. More importantly, those AI-determined low-risk patients could benefit substantially from postoperative adjuvant chemotherapies, while the high-risk patients may be spared further conventional chemotherapy due to extremely limited therapeutic benefits. These results shed light on the great potential of our AI model in detecting responders (up to ~42% among all SRCC patients in the current study) who would be more likely to benefit from chemotherapy. In this regard, as the management of GC continues to move toward a focus on precision medicine, our AI model could help patients avoid nonbeneficial conventional adjuvant therapies in favor of supportive care or novel treatment modalities. The strengths of AI may pave the way for individualized treatment-planning throughout chemotherapy regimen selection, response prediction, and long-term survival stratification. Furthermore, the utility of our model may also be extrapolated to the preoperative settings, where the model could offer help in predicting treatment response to neoadjuvant chemotherapies in confirmed SRCC patients.

A number of limitations should be noted in this study. First, this was a single-institutional study, and the model

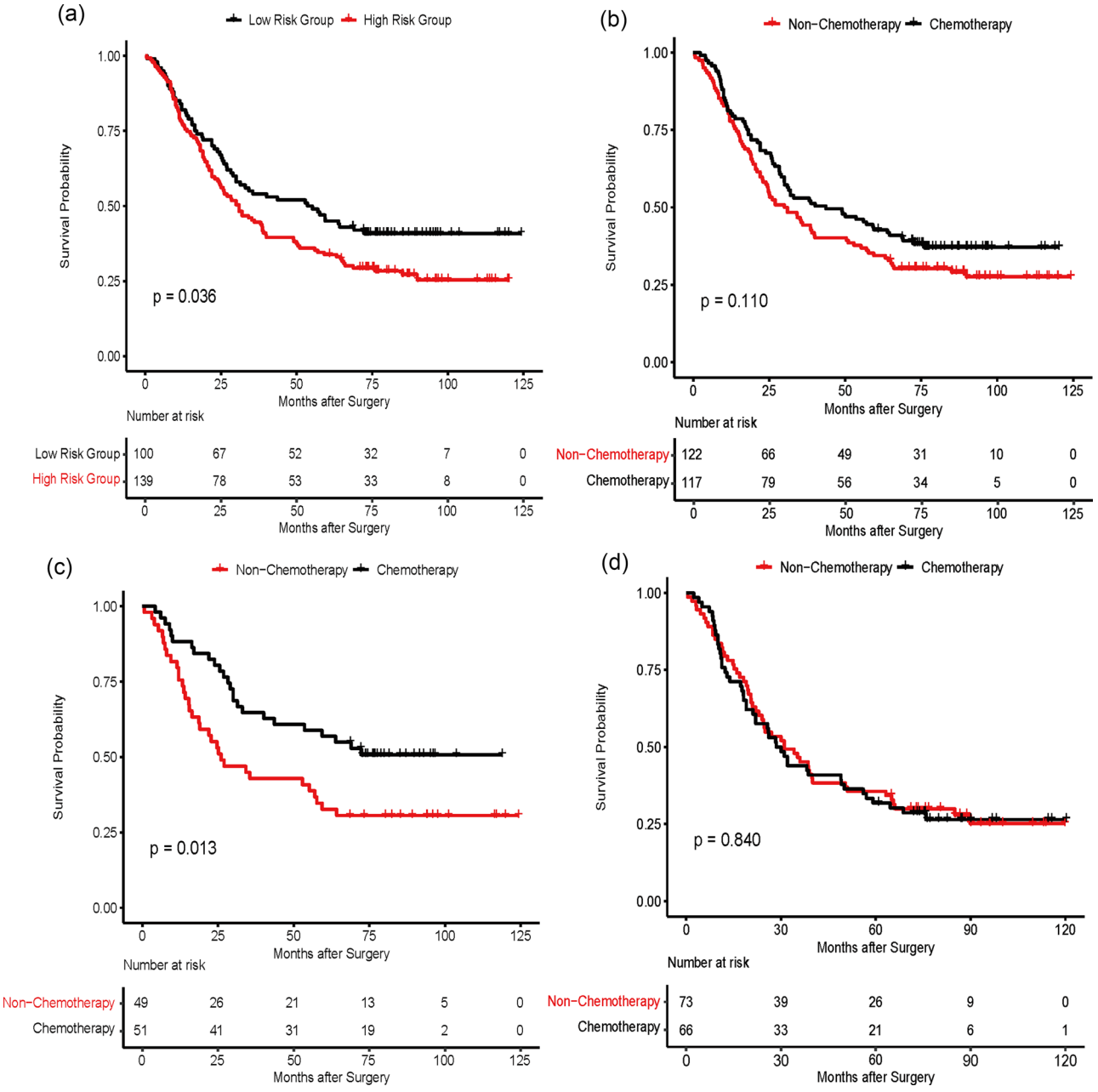

FIGURE 4 Survival curves of $Model_{AI}$ for stratifying overall survival and predicting chemotherapy response in advanced SRCC patients. (a) All advanced SRCC patients assigned in high- ($n = 139$) and low-risk ($n = 100$) groups according to $Model_{AI}$. (b) Chemotherapy outcomes of all the advanced SRCC patients. (c) Chemotherapy outcomes of advanced SRCC patients in AI-predicted low-risk subgroup. (d) Chemotherapy outcomes of advanced SRCC patients in AI-predicted high-risk subgroup. SRCC, Signet-ring cell carcinoma

should be validated on a larger multicenter dataset. Second, all patients included in the current study underwent curative surgical intent resection. Therefore, our findings may not apply to GC patients who are not candidates for primary resection. Third, the survival analysis was conducted in a retrospective manner, which to some extent had dampened the utility of our AI model as a predictor of the chemotherapy response, particularly in preoperative settings. Therefore, despite the promising results of our AI model in SRCC diagnosis and risk stratification, hope should be tempered until they are validated in further prospective studies. Fourth, although 3D ROIs covering the entire tumor might provide more information regarding tumor biology and heterogeneity. However, the annotation of the entire tumor in 3D is time-consuming, 2D ROIs on the single largest slice were analyzed for the sake of efficiency. Finally, only clinical and imaging data were combined in the AI model generated in this study. However, given the marked ability of AI in aggregating parallel data

streams, efforts should continue to be actively pursued to integrate more genomics and pathology information to further optimize the current model.

5 | CONCLUSIONS

In summary, based on preoperative CT images, we constructed a promising AI model, which demonstrated good performance for diagnosing SRCC in GC patients. The model also showed promise in stratifying patient prognosis and identifying advanced SRCC patients who can benefit from chemotherapy.

ACKNOWLEDGMENTS

This work was supported by the National Key R&D Program of China (2017YFC1309100, 2017YFA0205200), National Natural Science Foundation of China (91959130, 81971776, 81902437, 81771924, 61622117, 81671759, 81930053, 81527805, 91959205), the Beijing Natural Science Foundation (L182061, Z20J00105, JQ19027), Beijing Nova Program (Z181100006218046), 1.3.5 Project for Disciplines of Excellence, West China Hospital, Sichuan University, No. ZYJC21006, Post-Doctor Research Project, West China Hospital, Sichuan University (2018HXBH010), Project funded by China Postdoctoral Science Foundation (2019M653418, 2020T130449), Strategic Priority Research Program of Chinese Academy of Sciences (XDB 38040200), the Scientific Instrument Developing Project of the Chinese Academy of Sciences (YZ201672), and the Youth Innovation Promotion Association CAS (2017175).

CONFLICT OF INTEREST

The authors have no relevant conflicts of interest to disclose.

DATA SHARING AND DATA ACCESSIBILITY

The datasets used and analyzed in this study are available from the corresponding author on reasonable request.

REFERENCES

1. Bray F, Ferlay J, Soerjomataram I, Siegel RL, Torre LA, Jemal A. Global cancer statistics 2018: GLOBOCAN estimates of incidence and mortality worldwide for 36 cancers in 185 countries. *CA Cancer J Clin*. 2018;68(6):394–424. https://doi.org/10.3322/caac.21492
2. Chen W, Zheng R, Baade PD, et al. Cancer statistics in China, 2015. *CA Cancer J Clin*. 2016;66(2):115–132. https://doi.org/10.3322/caac.21338
3. Bosman FT, Carneiro F, Hruban RH, et al. *WHO classification of tumours of the digestive system[M]* World Health Organization, 2010.
4. Kwon KJ, Shim KN, Song EM, et al. Clinicopathological characteristics and prognosis of signet ring cell carcinoma of the stomach. *Gastric Cancer*. 2014;17(1):43–53. https://doi.org/10.1007/s10120-013-0234-1
5. Nie RC, Yuan SQ, Li YF, et al. Clinicopathological characteristics and prognostic value of signet ring cells in gastric carcinoma: a meta-analysis. *J Cancer*. 2017;8(17):3396–3404. https://doi.org/10.7150/jca.21017.
6. Chon HJ, Hyung WJ, Kim C, et al. Differential prognostic implications of gastric signet ring cell carcinoma: stage adjusted analysis from a single high-volume center in Asia. *Ann Surg*. 2017;265(5):946.
7. Golembeski CP, Genta RM. Signet-ring cell carcinoma in gastric biopsies: expecting the unexpected. *J Clin Pathol*. 2013;66(2):136–139.
8. Gullo I, Carneiro F, Oliveira C, Almeida GM. Heterogeneity in gastric cancer: from pure morphology to molecular classifications. *Pathobiology*. 2018;85(1-2):50–63.
9. Kim DY, Park YK, Joo JK, et al. Clinicopathological characteristics of signet ring cell carcinoma of the stomach. *ANZ J Surg*. 2004;74(12):1060–1064.
10. Machlowska J, Pucułek M, Sitarz M, Terlecki P, Maciejewski R, Sitarz R. State of the art for gastric signet ring cell carcinoma: from classification, prognosis, and genomic characteristics to specified treatments. *Cancer Manage Res*. 2019;11:2151.
11. Zhang L, Dong D, Zhang W, et al. A deep learning risk prediction model for overall survival in patients with gastric cancer: a multicenter study. *Radiotherap Oncol*. 2020;150:73–80.
12. Lambin P, Rios-Velazquez E, Leijenaar R, et al. Radiomics: extracting more information from medical images using advanced feature analysis. *Eur J Cancer*. 2012;48(4):441–446. https://doi.org/10.1016/j.ejca.2011.11.036
13. Bi WL, Hosny A, Schabath MB, et al. Artificial intelligence in cancer imaging: clinical challenges and applications. *CA Cancer J Clin*. 2019;69(2):127–157. https://doi.org/10.3322/caac.21552
14. Dong D, Zhang F, Zhong LZ, et al. Development and validation of a novel MR imaging predictor of response to induction chemotherapy in locoregionally advanced nasopharyngeal cancer: a randomized controlled trial substudy (NCT01245959). *BMC Med*. 2019;17(1):190. https://doi.org/10.1186/s12916-019-1422-6
15. Dong D, Fang M-J, Tang L, et al. Deep learning radiomic nomogram can predict the number of lymph node metastasis in locally advanced gastric cancer: an international multi-center study. *Ann Oncol*. 2020;31(7):912-920.
16. Zhang L, Dong D, Zhong L, et al. Multi-focus network to decode imaging phenotype for overall survival prediction of gastric cancer patients. *IEEE J Biomed Health Informat*. 2021;25(10):3933-3942.
17. Gillies RJ, Kinahan PE, Hricak H. Radiomics: images are more than pictures, they are data. *Radiology*. 2016;278(2):563–577. https://doi.org/10.1148/radiol.2015151169
18. Dong D, Tang L, Li ZY, et al. Development and validation of an individualized nomogram to identify occult peritoneal metastasis in patients with advanced gastric cancer. *Ann Oncol*. 2019;30(3):431–438. https://doi.org/10.1093/annonc/mdz001
19. Jiang Y, Wang H, Wu J, et al. Noninvasive imaging evaluation of tumor immune microenvironment to predict outcomes in gastric cancer. *Ann Oncol*. 2020;31(6):760-768. https://doi.org/10.1016/j.annonc.2020.03.295
20. He B, Dong D, She Y, et al. Predicting response to immunotherapy in advanced non-small-cell lung cancer using tumor mutational burden radiomic biomarker. *J Immunother Cancer*. 2020;8(2). https://doi.org/10.1136/jitc-2020-000550
21. Lao J, Chen Y, Li ZC, et al. A deep learning-based radiomics model for prediction of survival in glioblastoma multiforme. *Sci Rep*. 2017;7(1):10353. https://doi.org/10.1038/s41598-017-10649-8
22. Bibault JE, Giraud P, Housset M, et al. Deep learning and radiomics predict complete response after neo-adjuvant chemoradiation for locally advanced rectal cancer. *Sci Rep*. 2018;8(1):12611. https://doi.org/10.1038/s41598-018-30657-6

23. Aerts HJ, Velazquez ER, Leijenaar RT, et al. Decoding tumour phenotype by noninvasive imaging using a quantitative radiomics approach. *Nat Commun*. 2014;5:4006. https://doi.org/10.1038/ncomms5006
24. Peng H, Dong D, Fang MJ, et al. Prognostic value of deep learning PET/CT-based radiomics: potential role for future individual induction chemotherapy in advanced nasopharyngeal carcinoma. *Clin Cancer Res*. 2019;25(14):4271–4279. https://doi.org/10.1158/1078-0432.Ccr-18-3065
25. Ma Z, Fang M, Huang Y, et al. CT-based radiomics signature for differentiating Borrmann type IV gastric cancer from primary gastric lymphoma. *Eur J Radiol*. 2017;91:142–147. https://doi.org/10.1016/j.ejrad.2017.04.007
26. Zhang WH, Chen XZ, Liu K, et al. Outcomes of surgical treatment for gastric cancer patients: 11-year experience of a Chinese high-volume hospital. *Med Oncol*. 2014;31(9):150. https://doi.org/10.1007/s12032-014-0150-1
27. Chen H-N, Shu Y, Liao F, et al. Genomic evolution and diverse models of systemic metastases in colorectal cancer. *Gut*. 2022;71(2):322-332. https://doi.org/10.1136/gutjnl-2020-323703.
28. Japanese gastric cancer treatment guidelines 2010 (ver. 3). *Gastric Cancer*. 2011;14(2):113-123. https://doi.org/10.1007/s10120-011-0042-4
29. Lauren P. The two histological main types of gastric carcinoma: diffuse and so-called intestinal-type carcinoma. an attempt at a histo-clinical classification. *Acta Pathol Microbiol Scand*. 1965;64:31–49. https://doi.org/10.1111/apm.1965.64.1.31.
30. van Griethuysen JJM, Fedorov A, Parmar C, et al. Computational radiomics system to decode the radiographic phenotype. *Cancer Res*. 2017;77(21):e104-e107. https://doi.org/10.1158/0008-5472.Can-17-0339
31. He K, Zhang X, Ren S, Sun J. Deep residual learning for image recognition. 2016; arXiv:1512.03385.
32. Ronneberger O, Fischer P, Brox T. *U-Net: Convolutional Networks for Biomedical Image Segmentation*. Springer International Publishing; 2015:234–241.
33. Zhou Z, Sodha V, Siddiquee MMR, et al. Models genesis: generic autodidactic models for 3D medical image analysis. *Med Image Comput Comput Assist Interv*. 2019;11767:384–393. https://doi.org/10.1007/978-3-030-32251-9_42
34. Brown CE. *Coefficient of Variation. Applied Multivariate Statistics in Geohydrology and Related Sciences*. Springer; 1998:155–157.
35. Camp RL, Dolled-Filhart M, Rimm DL. X-tile: a new bio-informatics tool for biomarker assessment and outcome-based cut-point optimization. *Clin Cancer Res*. 2004;10(21):7252–7259. https://doi.org/10.1158/1078-0432.Ccr-04-0713
36. Liu S, Liu S, Ji C, et al. Application of CT texture analysis in predicting histopathological characteristics of gastric cancers. *Eur Radiol*. 2017;27(12):4951–4959. https://doi.org/10.1007/s00330-017-4881-1
37. Wang Y, Liu W, Yu Y, et al. Potential value of CT radiomics in the distinction of intestinal-type gastric adenocarcinomas. *Eur Radiol*. 2020;30(5):2934–2944. https://doi.org/10.1007/s00330-019-06629-3
38. Chen J, Cai R, Ren G, et al. Differences in clinicopathological characteristics and computed tomography findings between signet ring cell carcinoma and nonsignet ring cell carcinoma in early and advanced gastric cancer. *Cancer Med*. 2018;7(4):1160–1169. https://doi.org/10.1002/cam4.1417
39. Shu Y, Zhang W, Hou Q, et al. Prognostic significance of frequent CLDN18-ARHGAP26/6 fusion in gastric signet-ring cell cancer. *Nat Commun*. 2018;9(1):2447. https://doi.org/10.1038/s41467-018-04907-0
40. Chon HJ, Hyung WJ, Kim C, et al. Differential prognostic implications of gastric signet ring cell carcinoma: stage adjusted analysis from a single high-volume center in Asia. *Ann Surg*. 2017;265(5):946–953. https://doi.org/10.1097/sla.0000000000001793
41. Heger U, Blank S, Wiecha C, et al. Is preoperative chemotherapy followed by surgery the appropriate treatment for signet ring cell containing adenocarcinomas of the esophagogastric junction and stomach?. *Ann Surg Oncol*. 2014;21(5):1739–1748. https://doi.org/10.1245/s10434-013-3462-z
42. Comprehensive molecular characterization of gastric adenocarcinoma. *Nature*. 2014;513(7517):202-209. https://doi.org/10.1038/nature13480

SUPPORTING INFORMATION

Additional supporting information may be found in the online version of the article at the publisher's website.

How to cite this article: Li C, Qin Y, Zhang W-H, et al. Deep learning-based AI model for signet-ring cell carcinoma diagnosis and chemotherapy response prediction in gastric cancer. *Med Phys.* 2022;49:1535–1546. https://doi.org/10.1002/mp.15437